



Enhanced mechanical, crystallisation and thermal properties of graphene flake-filled polyurethane nanocomposites: the impact of thermal treatment on the resulting microphase-separated structure

Muayad Albozahid¹ · Haneen Zuhair Naji² · Zoalfokkar Kareem Alobad³ · Alberto Saiani⁴

Received: 10 May 2021 / Accepted: 8 July 2021 / Published online: 15 July 2021
© The Polymer Society, Taipei 2021

Abstract

The present work investigates the combined effect of the addition of graphite nanoplatelets (xGNPs) to polyurethane copolymer (PUC) and thermal treatment was employed. The PUC reinforced by xGNP were synthesized by in-situ polymerisation, which leads to an effective performance of the PUC/xGNP system. Meanwhile, X-ray diffraction (XRD) and Raman spectroscopy tests displayed the inter-spacing planar quality of xGNP nanofillers. The thermal stability of PUC was seen to increase with addition of xGNP. Additionally, the dynamic storage modulus (E') showed better performance after thermal treatment than in the untreated samples. However, a relationship between the microphase-separated morphology of PUC induced by thermal treatment and the addition of xGNP has been observed. Consequently, the crystallinity percentage increased after thermal treatment @ 80 °C for 4 days, presuming a re-ordering of amorphous hard segments during the heating in a packed microphase conformation. On the other hand, better dispersion and interaction of xGNP can play a crucial role in enhancing the thermal and mechanical properties, and thus a significant reinforcement for PUC. The tensile properties such as modulus and tensile strength showed significant enhancement with xGNP incorporation, while the elongation steeply dropped. On the contrary, a deterioration in modulus and tensile strength resulted from thermal treatment, likely due to the restacking of xGNP during segmental movement and thus increasing the amorphous phase rather than the crystalline phase. A modified Halpin–Tsai model was utilised to predict the mismatch between the empirical and theoretical results. Consequently, the findings displayed the divergence of the nanocomposite modulus of PUC with greater amounts of xGNP nanofillers.

Keywords Polyurethane copolymer · PUC · Microphase-separated structure · Thermal and mechanical properties · Halpin–Tsai models

Introduction

Polyurethane copolymer (PUC), classified as a type of thermoplastic polyurethane, has attracted tremendous attention among the research community as well as in industrial fields. Commonly, polyurethane is considered one of the most versatile plastic materials derived from different kinds of raw chemicals such as MDI. The MDI is responsible for hard domains and polyether or polyester polyol which represents the soft domain and thus reflects the PUC flexibility that is needed for different applications [1–5]. Phase separation between hard and soft segments, as well as hydrogen bonding that exists between urethane bonds, have a high impact on the resultant mechanical properties of this polymer [6–8].

Polymer nanocomposites (PNCs) are a good candidate for use instead of virgin polymers. They have a massive interfacial area between the polymer matrix and the additives

✉ Muayad Albozahid
moayad.zahid@uokufa.edu.iq

¹ Department of Materials Engineering, Faculty of Engineering, University of Kufa, Najaf, Iraq

² Department of Chemical Engineering, Faculty of Engineering, University of Babylon, Hilla, Iraq

³ Department of Polymers Engineering and Petrochemical Industries, Faculty of Materials Engineering, University of Babylon, Hilla, Iraq

⁴ Department of Materials and Manchester Institute of Biotechnology, School of Natural Sciences, Faculty of Science and Engineering, The University of Manchester, Manchester, UK

due to the minute thickness of those materials. Thus, this huge interfacial area creates a significant volume fraction of polymer in close proximity to the interface with behaviour that differs entirely from the original properties of the pure polymer. This affects the properties substantially, even at low concentration of nanoscale filler [9, 10]. However, the mixing method is important in order to gain an optimised interface through enhanced dispersion and distribution of nanofillers within polymer matrices [10, 11]. The dispersion and distribution of nanofillers within polymers is the main challenge in the fabrication of nanocomposites and substantially influences their final performances. Since most polymer nanocomposites are synthesised using in situ polymerisation, solution mixing and melt compounding. Solution mixing includes the addition of solvent to dissolve the polymer and the dispersion of the nanofiller into the polymer–solvent solution. When the mixing is complete, the polymer nanocomposites can be obtained by abstracting the solvent through casting and drying. While, melt compounding utilises high temperatures applied to a mixing machine. Generally, melt compounding can apply high shear forces by rotating screws or rotors to disperse the nanofillers in a molten polymer matrix [12–14].

However, the in-situ polymerisation method is the most effective method to disperse nanofillers within polymer matrices from the literature [15, 16]. The nanofillers and monomers are polymerised together, thus leading to more effective interaction between the matrix and nanofillers. Nanocomposites prepared using this method often possess enhanced mechanical properties and show much lower percolation thresholds compared to the solution mixing and melt compounding methods [17, 18]. PUC as a thermoplastic copolymer material was modified to compensate for the poor properties demanded in various extensive applications [19–22]. That is to say, most types of improved PUC composites in the literature are based on different raw materials, such as MDI [23] or TDI [24], as primary chemicals, which are responsible for the hard phase formation. Besides that, polyether [25, 26] and polyester polyol [27] were responsible for the soft phase. The change in the morphology (micro-phase separation of PUC) imposed by the annealing might exhibit a positive or detrimental effect on the performance of PUC with added nanofillers reaching the desired properties [28, 29]. Recently, the chain extender types that have been used in PUC production have varied. However, few attempts have been made to examine the use of different chain extenders such as 1,5 PD accompanied with the effect of thermal treatment on the properties of PUC filled with xGNP nanoparticles. On this basis, the current study will focus on the relationship between the resulting properties and structural configuration of resultant PUC/xGNP nanocomposites before and after annealing treatment. Herein, 1,5 pentane-diol was exploited to fabricate this PUC via a

two-step polymerisation (pre-polymer) approach with different weight contents of xGNP.

Graphene nanoplatelets (xGNPs) are two-dimensional atomic layers of sp^2 hybridised carbon atoms with extraordinary electrical, mechanical and thermal properties. These properties lead to potential applications relevant to sensors, storage components or even packaging applications [30, 31]. As previously reported, studies have been conducted on xGNPs as a reinforcement additive with different types of materials such as polypropylene [32, 33], polyethylene [34], PVA [35], PC [36], and so on. Meanwhile, thermosetting polymeric materials were also tailored by incorporating various kinds of xGNP, such as epoxy [10]. The authors An Huang et al. [37] reported various characterisation analyses based on the addition of graphite particles to thermoplastic polyurethane (TPU) using a novel dispersion method. These measurements include thermal behaviour including DSC thermograms, SEM morphology evaluation, tensile performance and rheology test. The researchers found that CO_2 usage would consolidate the dispersion quality and prevented the graphite from becoming aggregated at the loading (3 Wt.%). Good tensile and rheology results were obtained by employing this novel approach. Furthermore, the xGNP were considered to be an excellent reinforcement material for improving the shape-memory properties of PU, as has been suggested by another previous study [38]. Remarkable enhancements were observed for PU/GNP samples regarding dynamic storage modulus as well as glass transition temperature. However, xGNPs were used in this study with a minimum concentration of 0.8%.

In this article, the evaluation of the effective reinforcement of xGNP dispersion within PUC was conducted through a new route of in situ polymerisation method. For this purpose, wide range of loading contents of xGNP was inserted during this fabrication method. Thus, a comparison between experimental and theoretical results will be evaluated based on tensile performance using modified Halpin–Tsai equations.

Experimental set-up

Materials

Polyurethane block copolymer (PUC) with a relatively high amount of hard segments was used in this work. The PUC was synthesised from polyether polyol based on a polyethylene glycol-block-polypropylene glycol-block-polyethylene glycol structure (EO-PPO-EO) as a soft segment with $M_n = 2000$ g/mol and functionality of 2.0. The isocyanate, MDI (4,4'-methylenebis phenyl isocyanate) was purchased as solid flakes with a solution-based chain extender (1,5 pentane-diol). A catalyst of 1,4-diazabicyclo[2.2.2]octane

(DABCO-S) and N,N dimethylene-acetamide (DMAC) solvent were also used as solvent for the PUC-based solution. All of these chemicals were supplied by Sigma-Aldrich. The M-grade xGNP (graphene nanoplatelet) nanofillers were purchased from Lansing, MI USA – XG sciences, Inc., and were characterised with an average thickness of 6–8 nm (18–24 layers of graphene) and possessed a nominal surface area of 120 to 150 m²/g.

Preparation of graphite nanoplatelets (xGNPs)

In order to minimise the tendency of xGNP clusters to aggregate, the xGNP powder was initially dried using an aluminium pan inside an oven; the thickness of the xGNPs was around 5 mm. After 24 h, the dried xGNPs were left to cool down at room temperature in a vacuum atmosphere to minimise reaction with the ambient atmosphere. Afterwards, xGNP powder was dissolved with DMAC solvent with a solution concentration of 2 g/ml. Lastly, this xGNP solution was placed in a round container and sealed tightly and inserted in the ultrasound bath machine for 2 h to obtain highly dispersed xGNP before usage for in-situ polymerisation of PUC synthesis.

Approach to PUC synthesis

A two-step polymerization method was used to synthesize the PUC polymer as reported in previous study [39]. Briefly,

a laboratory flask was used with a nitrogen inlet since the first step contained the reaction between MDI and polyol in an oil bath at a temperature of 80 °C chemical stoichiometry equivalent to a 6:1 ratio. After 10 min later from the addition of MDI, the polyol was inserted gradually and the reaction was left for at least 2 h with vigorous mechanical stirring to obtain the pre-polymer (MDI bonded with polyol) with excess MDI. In the second step, the chain extender (CE) of 1,5 Pentane-diol was added. Then, continuous mixing of the mixture with drop-wise addition of the prepolymer was performed. After the drop-wise addition of the prepolymer, the reaction continued with stirring for at least two hours until completion. The final PUC solution was kept in glass jars for the next step of nanocomposites synthesis.

Preparation of PUC/ xGNP nanocomposites

The xGNP solution was mixed with prepolymer during the PUC in-situ polymerisation process. When the synthetic process finished, the PUC/xGNP nanocomposite solution was poured into rectangular cavity moulds and put in a furnace to dry in order to obtain solid sheets. The PUC /xGNP pieces were dried in a vacuum oven at 80 °C for 24 h before sample fabrication. The injection moulding was performed to make test samples using is a Haake Minijet II (Thermoscientific). The machine is connected with a barrel controlled by a control panel to set the barrel temperature at 200 °C with a mould temperature of 50 °C. The injection pressure of the

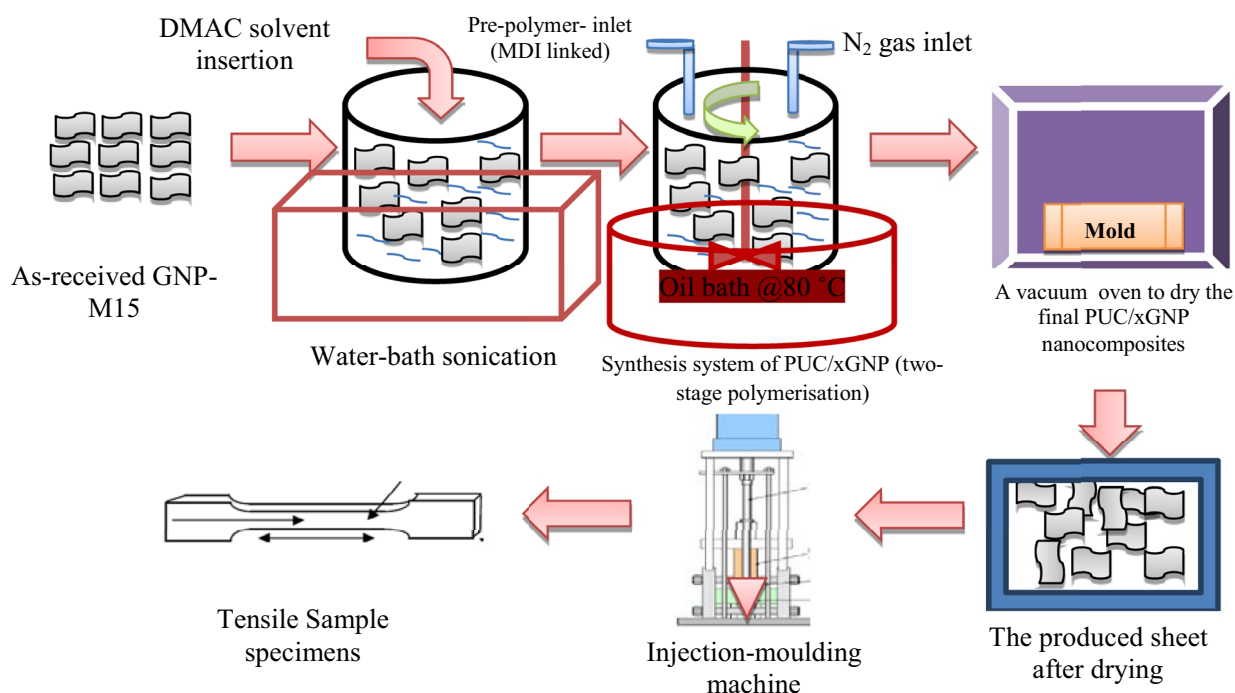


Fig. 1 Schematic representation of the PUC/xGNP nanocomposite fabrication steps using a sonication bath and in-situ polymerised system with an oven and nitrogen inlet to maintain the inert atmosphere environment inside the reaction vessel

molten PUC/xGNP material was set at 500–1200 bar for 10 s in addition to the holding pressure being set at 400–1000 bar for an additional period of 5–10 s before the sample was removed. The fabrication route of PUC/xGNP samples is shown in Fig. 1. The final samples of PUC/xGNP were injected samples as tensile-shape samples as shown in Fig. 2.

Measurements and characterisations

X-ray diffraction (XRD)

An X-ray diffraction (XRD) machine (X'Pert X-ray diffractometer) was used alongside a Cu K α radiation source ($\lambda = 1.542 \text{ \AA}$) at a generator voltage of 35 kV and a generator current of 25 mA to identify the basic xGNP structure. The crystallinity of the PUC/xGNP nanocomposites was also tested to reveal the intercalation/exfoliation pattern by using injection-moulded samples with a rectangular shape measuring 1 mm \times 0.5 mm.

Raman spectroscopy

The Raman spectrum was obtained using a Renshaw InVia Raman spectrometer with a laser wavelength of 514 nm and a $\times 100$ objective lens. The xGNP and graphite powder was put on a glass slide to investigate the quality of xGNP compared to graphite as a base material. These samples were handled carefully to prevent distortion of the laser signal during the test.

Thermogravimetric analysis (TGA)

A TGA analyser (Q-500, TA Instruments) was utilised to investigate the thermal stability of PUC/xGNP nanocomposites with a heating rate of 10 $^{\circ}\text{C}/\text{min}$ under an N_2 gas

atmosphere. The degradation temperature (T_{onset}) was determined from weight loss data. In addition, the derivative weight curves were employed to measure both the first and second stages of degradation of PUC.

Differential scanning calorimetric analysis (DSC)

The thermal properties of PUC/xGNP nanocomposites were investigated using an auto-sampler (Q100, TA Instruments) and the Indium calibration standard. The weight of the samples was around 7–11 mg, and the custom type protocol that was employed consisted of a cool/heat/cool/heat sequence with a heating range of $-90 \text{ }^{\circ}\text{C}$ to $200 \text{ }^{\circ}\text{C}$ and a rate of $10 \text{ }^{\circ}\text{C}/\text{min}$ under an N_2 atmosphere.

Dynamic mechanical thermal analysis (DMTA)

Dynamic mechanical analysis of the PUC and its nanocomposites was conducted using TA Instruments equipment (Q800 series DMTA) at a heating rate of $3 \text{ }^{\circ}\text{C}/\text{min}$ in a single-cantilever mode. The samples' size was $30 \text{ mm} \times 5 \text{ mm} \times 1.6 \text{ mm}$ (by cutting the middle part of the tensile specimen), and it was heated from -120 to $150 \text{ }^{\circ}\text{C}$ for at least 3 samples. The sample was deformed at a constant amplitude of $15 \text{ }\mu\text{m}$ and an experimental frequency of 1 Hz.

Mechanical properties

The tensile properties of the neat PUC and PUC/xGNP nanocomposites were measured using a universal testing machine (an Instron 1122) inside a controlled room (temperature $\sim 25 \text{ }^{\circ}\text{C}$, humidity $\sim 50\%$, with a crosshead speed of $10 \text{ mm}/\text{min}$. The dumbbell-shaped test specimens were moulded (by tensile test) according to the ISO 527-2 1BA

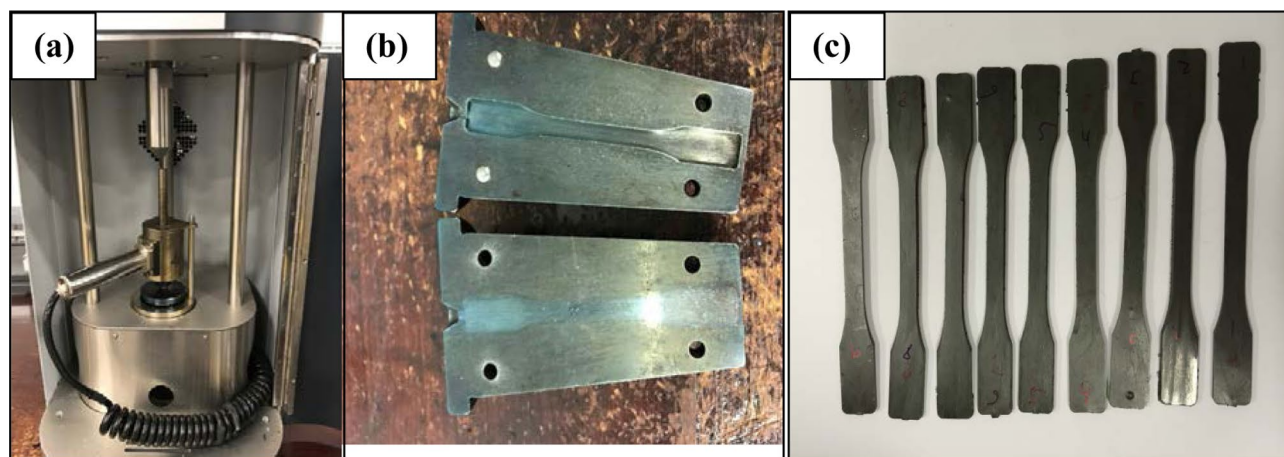


Fig. 2 PUC/xGNP sample tensile preparation processes, (a) the injection moulding machine, (b) the tensile specimen mould, and (c) the final shape of PUC/xGNP samples

standard. The samples were kept for 24 h before testing and at least 5 samples were tested and their average results taken, with a load cell of 0.5 kN and a distance between grips of 55 mm.

Results and discussion

XRD and raman spectroscopy of xGNP

The XRD pattern and Raman spectroscopy of the xGNP flakes compared to graphite as a reference material are illustrated in Fig. 3. The XRD characteristic peaks of pristine graphite indicate the intense diffraction peaks at 26.52° and 54.64° , which correspond to the reflections of the basal planes of (002) and (004) of xGNP with d-spacing of 1.73 nm and 0.95 nm, respectively [40, 41]. This was calculated according to the Bragg equation via wave length = 1.5419 nm. A slight shift was observed in the 2θ values for xGNP particles, proving the increase in inter-gallery spacing due to the exfoliation process. The xGNP structure was also reported by Jin Lin et al. with similar expected diffraction peaks showing highly exfoliated graphite nanoplatelets [42]. Furthermore, the Raman spectrum showed the basic crystallographic structure of xGNP corresponding to graphite as a reference to elucidate the differential variations. The most prominent feature of these materials is related to the first-order peak (G band) at a wave number of 1636 cm^{-1} and relatively high intensity. In addition, surface defects and disorder in the basal structure of these nanofillers showed at the band D, with the Raman position at approximately 1300 cm^{-1} . However, the 2D band

represented the second-order status of graphitic materials and lay between 2500 cm^{-1} to 2800 cm^{-1} . This Raman shift can reflect several quality characterisations of these nanofillers, owing to the ratio between the D and G bands [32, 41].

Thermal stability of PUC/xGNP nanocomposites

Figure 4a displays the normal TGA curves of pure PUC and its nanocomposites with xGNP to determine the variation in its thermal stability. Initially, the weight loss at 100°C could result from the water evaporation that was found in the samples [38, 43]. It was also observed that the onset temperature (T_{onset}) of pure PUC started at a temperature of around 295°C . Compared to pure PUC, the PUC/xGNP samples showed a good enhancement in thermal stability ($\sim 305^\circ\text{C}$), except the sample with xGNP loading at 15 Wt.%. Such an improvement in the thermal stability of PUC resulted from the advantage of high thermal stability of added xGNP with good attachment with PUC chains [44, 45]. Interestingly, the average constant weight losses of pure PUC and PUC/xGNP nanocomposites at $T_{0.05}$ (onset temperature) were observed to increase. This result can provide evidence of the quality of the PUC/xGNP nanocomposites produced. Meanwhile, the percentage of residual weight at 600°C displayed a large amount of values, particularly for higher concentrations (8 Wt.% and 15 Wt.%). The residual weight tended to increase from 8.9433% for pure PUC to 16.75% and 19.88% of PUC containing (8–15) Wt.% of xGNP, respectively. Overall, all PUC filled with xGNP exhibited better thermal stability performance due to the high stability of the xGNP nanofillers, which tended to act as a good barrier due to the tortuous path effect. This tortuous effect prevented the escape of all of

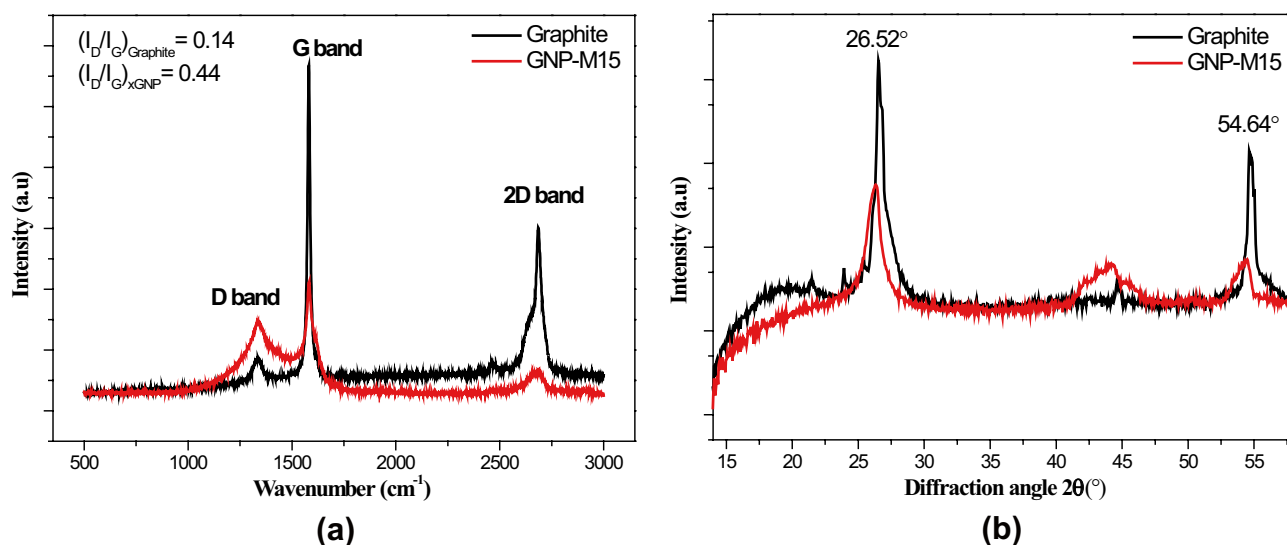


Fig. 3 Characterisation of xGNP nanoplatelets compared to graphite: (a) XRD pattern and (b) Raman spectrum

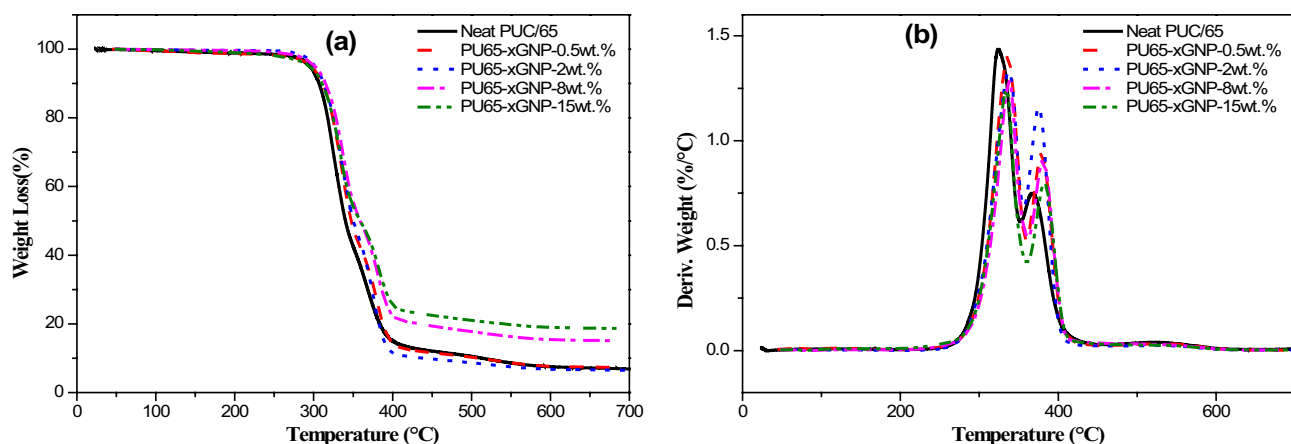


Fig. 4 TGA curves (10 °C/min) of PUC/xGNP nanocomposites compared to pure TPU: (a) TGA curves, (b) DTG curves

the gases generated during the heating process and released from the samples [46, 47].

Figure 4b shows the DTG curves to detect the rate of weight degradation of PUC upon temperature increase. In general, the DTG curves of PUC and their nanocomposites consist of a two-stage mechanism of thermal degradation. The first stage constitutes the dissociation of urethane linkage, converting to isocyanate and alcohol. Conversely, the second stage of degradation is associated with the mass loss of soft segments [28, 40]. However, by adding xGNP, these temperatures are shifted to a higher value, owing to the degradation inhibition effect of xGNP [48].

DSC Thermograms of PUC/xGNP nanocomposites

In order to further study the thermal behaviour (especially melting temperature (T_m) and crystallisation temperature (T_c) of PUC and PUC upon the incorporation of xGNPs, thermal investigation was conducted using DSC thermograms. The crystallinity was also calculated with respect to morphology change due to microphase separation induced by xGNP and thermal treatment. The DSC scans were conducted with various PUC nanocomposites containing xGNP at different weight loadings. In the first heating curves, as shown in Fig. 5, the endothermic peaks related to melting temperature (T_m) occurred around 171 °C for pure PUC and then rose to 175 °C for PUC containing xGNP at percentages of 0.5 Wt.% and 2 Wt.%. However, this T_m was seen to fall at greater loadings (8 Wt.% and 15 Wt.%) and T_m is almost recorded at 165 °C–170 °C, respectively. This reduction in T_m values could be related to the incapability of the melt-mixing process to achieve better dispersion and thus good interaction between the xGNP and PUC chains to gain better thermal properties. In addition, a sharp and abrupt endothermic peak of T_m was observed for the second heating scan due to the removal of thermal history, followed by

a sufficient period of time to re-crystallise all samples at a constant cooling rate [49, 50].

The broader endothermic peaks refer to the dissimilarity of the PUC microphases that formed even though strong crystallisation peaks indicate a wide range of crystal size domains [51–53]. The T_m values started from 176 °C for pure PUC and increased to 184 °C for xGNP-filled PUC at two concentrations of 0.5 Wt.% and 2 Wt.%, then decreased to 177 °C beyond this limit. Furthermore, the crystallisation behaviour during cooling revealed that crystallization of the T_c of pure PUC ~ 123 °C began earlier, rising to 127 °C, 132 °C, 138 °C and 142 °C of PUC containing xGNP at 0.5, 2, 8 and 15 Wt.%. This phenomenon is due to the action of xGNPs as nucleation sites during the cooling process [47, 51, 52], which facilitates crystal formation of hard domains (HDs). This finding was also concluded in the study by Jun Bian et al. [46], who found that the T_c of nanocomposites containing MEGO nanofillers would act as positive heterogeneous nucleation sites and thus trigger the early crystallisation process within the cooling scan. There are more nucleation locations as xGNP increased, but the mobility and diffusion of the PUC chains is also reduced, restricting the probability of crystallites growth of PUC.

In order to quantify the performance of both pure PUC and its nanocomposites during thermal treatment, a thermal investigation was carried out for PUC filled with xGNPs to reveal their response to the microphase separation process that could occur within two phases of PUC (hard and soft phases) which include xGNP nanofillers. A comparison of the thermal properties relevant to both T_m and T_c was undertaken to investigate untreated and thermally treated PUC nanocomposites. As was already known, the phase-separated PUC showed better performance in terms of thermal and mechanical properties compared to untreated pure PUC [54, 55]. A high quality xGNP nanofiller used in polymer matrices is not the crucial factor in order to achieve greater

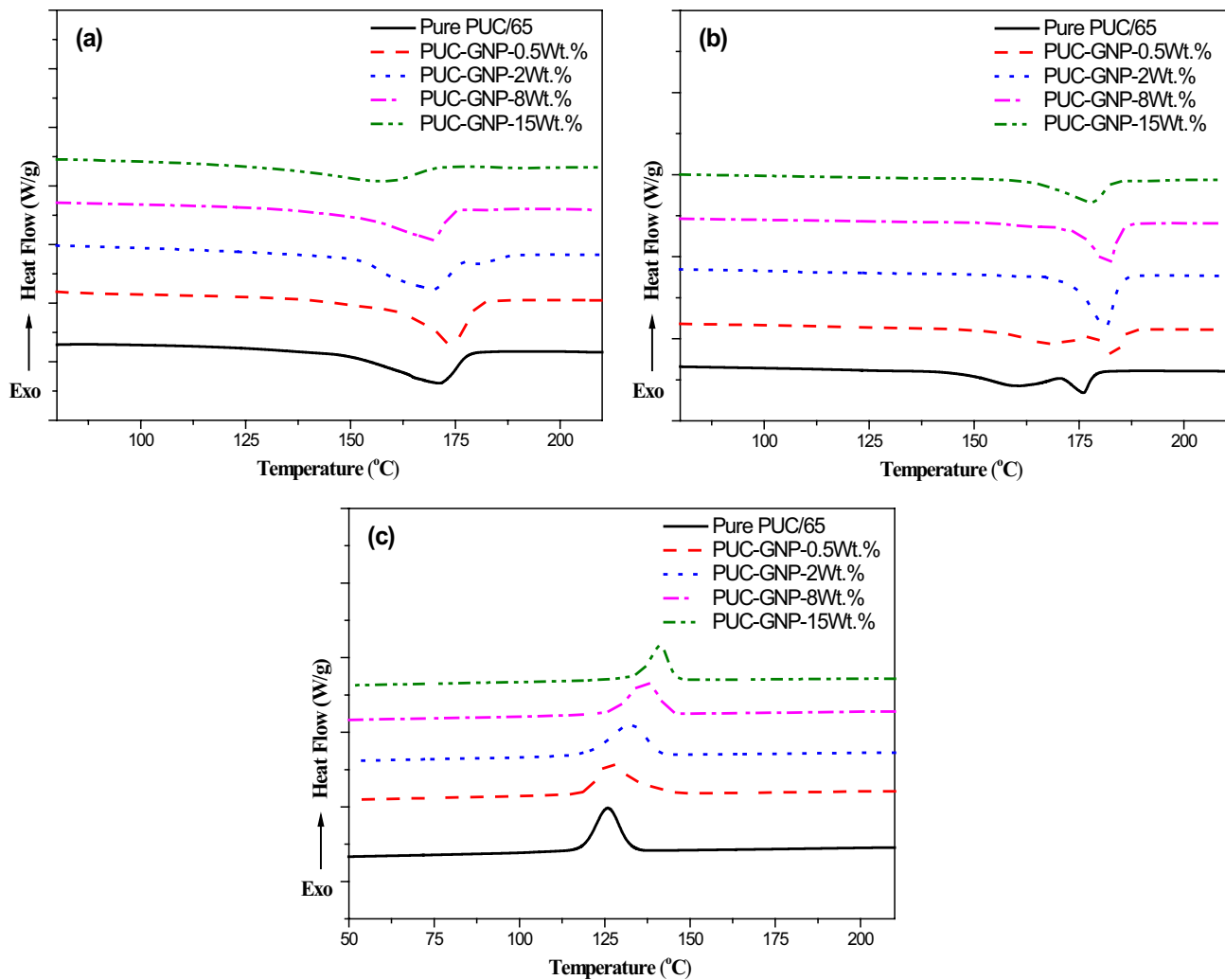


Fig. 5 Thermal behaviour (heating rate of 10 °C/min) of PUC/xGNP nanocomposites compared to pure PUC: (a) first heating scan, (b) second heating scan, and (c) cooling scan

performance or even multifactorial polymer nanocomposites. The challenge throughout incorporation of such nanofillers is obtaining sufficient interaction or adhesion between both surfaces of nanofillers and polymer chains [48]. Thus, better load transfer might occur during load exposure. Moreover, the problem is studied in the present work in order to understand whether or not it affects the final properties of PUC nanocomposites.

Figure 6 illustrates the thermal performance of PUC/xGNP nanocomposites after thermal treatment corresponding to neat PUC. Generally, both melting and crystallisation temperatures (T_m , T_c) seem to be improved after thermal treatment, reaching 183 °C and 142 °C for T_m and T_c , respectively. On the contrary, the T_m tended to reduce beyond 2 Wt.% of the xGNP limit and were ~176 °C and ~178 °C for loadings of 8 Wt.% and 15 Wt.%, respectively. In comparison, the T_m of pure PUC was 174 °C, owing to the

assumption of greater disordering of HDs due to the xGNPs restacking during thermal treatment. Nonetheless, these variations were seen only for the T_m of thermally treated PUC nanocomposites in the second heating scan. This restacking of xGNPs could lead to reduced efficiency of the interaction at the interfacial surfaces of xGNP and PUC chains [48], and thus, lower effectiveness in terms of stress transfer, resulting in a reduction in the final performance of xGNP/PUC nanocomposites [56, 57].

While T_m reduces at higher amounts of xGNP, the crystallisation peaks (T_c) of the nanocomposite samples were slightly increased, proving that xGNP nanofillers act as a nucleation agent at any loading. These results are in agreement with other previous works [56, 58, 59]. For example, Liang et al. found that when GNP was incorporated in polypropylene polymer, it could play a role in heterogeneous nucleation, leading to an increase in the degree of

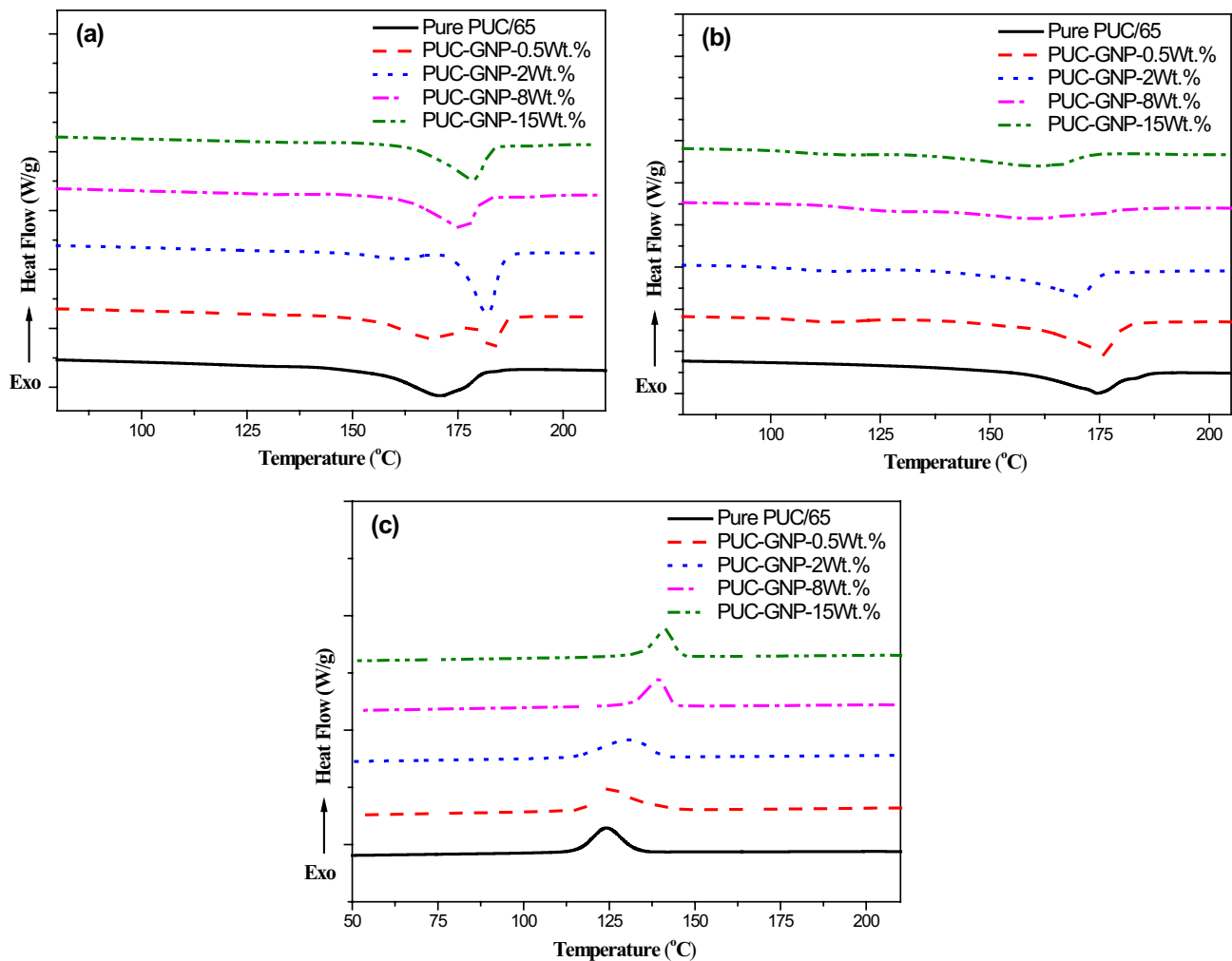


Fig. 6 Thermal behaviour (heating rate of 10 °C/min) of thermally treated PUC/xGNP nanocomposites compared to pure PUC: (a) first heating scan, (b) second heating scan, and (c) cooling scan

crystallinity, and to improve the inherent stiffness of the resultant systems, particularly at relatively low GNP loading.

Crystallinity, X_c , is a key point for PUC/xGNP nanocomposites, which can be determined using a second heating scan after removing all thermal history from the first scan and according to the equation of crystallinity obtained from previous studies [41, 52, 60]:

$$X_c = \frac{\Delta H_m}{(1 - \Phi)\Delta H_{100\%}} \quad (1)$$

The degree of crystallinity of the pure PUC and its counterparts containing xGNP increased from 13.63% to 15.14%, 16%, and 15.9% for PUC nanocomposites containing 0.5, 2, 8 and 15 Wt.% of xGNP, respectively. The hindrance of the crystallinity of PUC upon xGNP addition was remarkably seen at a loading of 15 Wt.%, reaching 12.4%. As indicated, the best values of crystallinity of

PUC/xGNP nanocomposites were at 0.5 and 2 Wt.% xGNP incorporation. This indicated a decline in the volume of crystals formed within the hard segments of PUC, which confirmed the hypothesis of xGNP aggregation. On the other hand, the counterparts of those samples after thermal annealing exhibited a slight decrease in crystallinity percentage, except at a loading of 15 Wt.% of xGNP. The microphase-separated structure was suppressed by nano-fillers and prevented the HDs from arranging themselves in uniform patterns [61]. It was reported by Bourque et al. that the increase in crystallinity with the addition of xGNP has a limit. The researchers found that after 5% of xGNP the crystallinity tended to decrease, due to the assumption of the diffusion barrier effect by xGNP and thus higher disruption to the ordering of chains, even though the presence of xGNPs encouraged the creation of nucleation sites [51, 62].

DMTA analysis of PUC/xGNP nanocomposites

The dynamic mechanical properties of PUC/xGNP nanocomposites in comparison with pure PUC were calculated using a DMTA instrument. The storage modulus (E') and loss tangent ($\tan\delta$) as a function of temperature ranging between $-90\text{ }^{\circ}\text{C}$ and $150\text{ }^{\circ}\text{C}$ are given in Fig. 7. All data for E' and $\tan\delta$ at different temperatures are shown in Table 1. With the addition of xGNP, the E' of the PUC nanocomposites increased remarkably for all loadings. The E' enhancement can be attributed to the high modulus of xGNP that was added [63, 64]. Meanwhile, an improvement in E' was exhibited by several magnitudes at the temperature below the T_g (glassy region) of HDs. A strong filler-matrix interaction can give more restriction for PUC chains; since the addition a small amount of xGNP can increase the microphase separation of PUC [65, 66]. At room temperature, a clear decrease in E' values of PUC/xGNP behaviour was exhibited prior to thermal treatment of PUC/xGNP samples

compared to their counterparts before this treatment. This trend indicates the aggregated xGNPs led to decrease the aspect ratio and thus weak interfacial interaction between the filler and polymer [67]. That is to say, microphase separated morphology can be restricted due to this phenomenon. However, the subsequent response becomes closer and even plateaus at the temperature above the T_g of HS (rubbery region) due to the enhanced mobility of both the soft and hard segments. This reveals the substantial mobility of the PUC segments including both HDs and SDs with increasing temperature [68]. In fact, the thermal treatment presumably exhibited lower values of E' due to the possibility of a huge aggregation of nano-scale fillers (xGNP) which preferred to locate themselves in the hard-phase regions rather than soft-phase regions, consequently preventing the effective load transition from hydrogenbonded PUC chains to xGNP clusters [69, 62].

On the other hand, the prominent $\tan\delta$ showed a certain shift in its values to lower magnitude with respect to pure

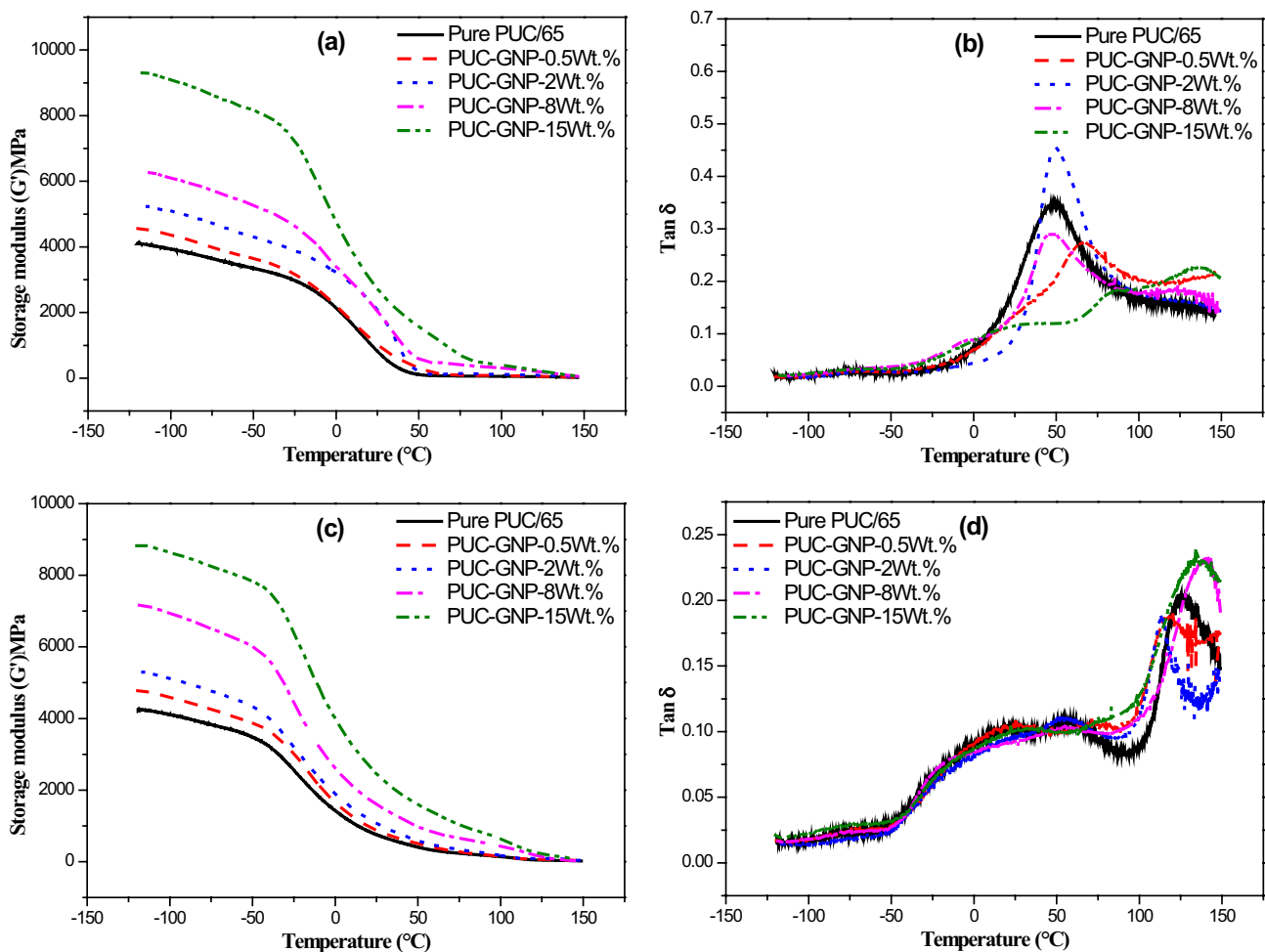


Fig. 7 Semi-log DMTA storage moduli and $\tan\delta$ versus temperature data of pure PUC and their nanocomposites after thermal treatment (annealed at $80\text{ }^{\circ}\text{C}$ for 4 days)

Table 1 Overall DMTA results of xGNP-based PUC nanocomposites

Sample	E' @ -100 °C		E' @ 25 °C		E' @ 100 °C		Tan δ		T _g @ Tan δ	
	Non-annealed	Annealed	Non-annealed	Annealed	Non-annealed	Annealed	Non-annealed	Annealed	Non-annealed	Annealed
Pure PUC	3132 ± 43	4347 ± 112	1505 ± 65	1543 ± 79	99 ± 3.2	210 ± 25	0.3 ± 0.06	0.11 ± 0.002	63 ± 2.3	67.8 ± 1.9
PUC-xGNP-0.5	4584 ± 115	4311 ± 163	2440 ± 45	1823 ± 65	80 ± 4.3	174 ± 36	0.71 ± 0.3	0.14 ± 0.01	56.4 ± 0.6	74 ± 3.8
PUC-xGNP-2	5014 ± 98	6001 ± 38	2115 ± 38	1056 ± 20	108 ± 9.5	170 ± 12.5	0.58 ± 0.17	0.12 ± 0.008	51 ± 1.1	56 ± 0.7
PUC-xGNP-8	5455 ± 203	7088 ± 287	2280 ± 176	1630 ± 172	295 ± 22	460 ± 30	0.41 ± 0.16	-	49 ± 0.7	-
PUC-xGNP-15	9160 ± 90	9308 ± 216	2570 ± 112	2666 ± 149	380 ± 28	690 ± 111	-	-	-	-

PUC. This also implies the disruption that took place in the 3D network structure of PUC/xGNP nanocomposites [70]. The tan δ peak represents the transition temperature (T_g) of the produced PUC nanocomposite materials. Thus, an improvement in T_g has been obtained from DMTA analysis, which is mainly attributed to the better dispersion of exfoliated high modulus xGNP particles and strong interconnection with the effective chains. This observation is particularly the case in the hard phase of PUC, resulting from the inter-molecular forces such as hydrogen bonding [67]. Similarly, a study was conducted by [64], who found that interfacial interaction would restrict the mobility of PUC chains. On the contrary, the dissipation factor (tanδ) showed a low magnitude when the nanocomposite samples were annealed. This result implied the assumption of restacking xGNP during the attempt of hard segments to be rearranged in a packed or ordering pattern. This could also be affected by the disruption of microphase separation in regions possessing large amounts of aggregated xGNP [28]. Such DMTA findings match with DSC results when crystallinity is calculated.

Tensile properties of PUC/xGNP nanocomposites

For a comparative study of xGNP-filled PUC nanocomposites before and after thermal treatment, the tensile behaviour of PUC when xGNP was incorporated using in-situ polymerisation displayed outstanding improvement compared to pure polymer. These enhancements in tensile properties such as tensile modulus and yield strength were from stress-strain curves, as shown in Fig. 8. Several factors affect the efficiency of this property, including xGNP dispersion as well as interfacial compatibility between xGNP and PUC polymer [57, 71]. To some extent, the annealed PUC/xGNP samples exhibited slightly lower values in both tensile modulus and tensile strength. This occurred as a result of the suppression of the microphase-separated structure of PUC due to the restacking of xGNPs. Reduced tensile performance for annealed specimens is found to correspond to untreated counterpart samples. The overall addition process of xGNPs to untreated PUC significantly increases the tensile performance with the limit of 8 Wt.% of xGNP, while at 15 Wt.% of xGNP, the tensile properties relatively reduced the tensile response. This deterioration is also in agreement with the results of DSC through crystallinity measurements [47]. The reduction occurs with the ultimate strength at 8 Wt.% due to the nanofillers restacking, which suppresses the strain hardening during tensile testing [40]. It is clear that elongation at break showed minimum magnitude for all nanocomposites before and after treatment.

The efficiency of stress transfer can significantly affect tensile properties due to the action of better compatibility between filler and polymers and vice versa [41]. This

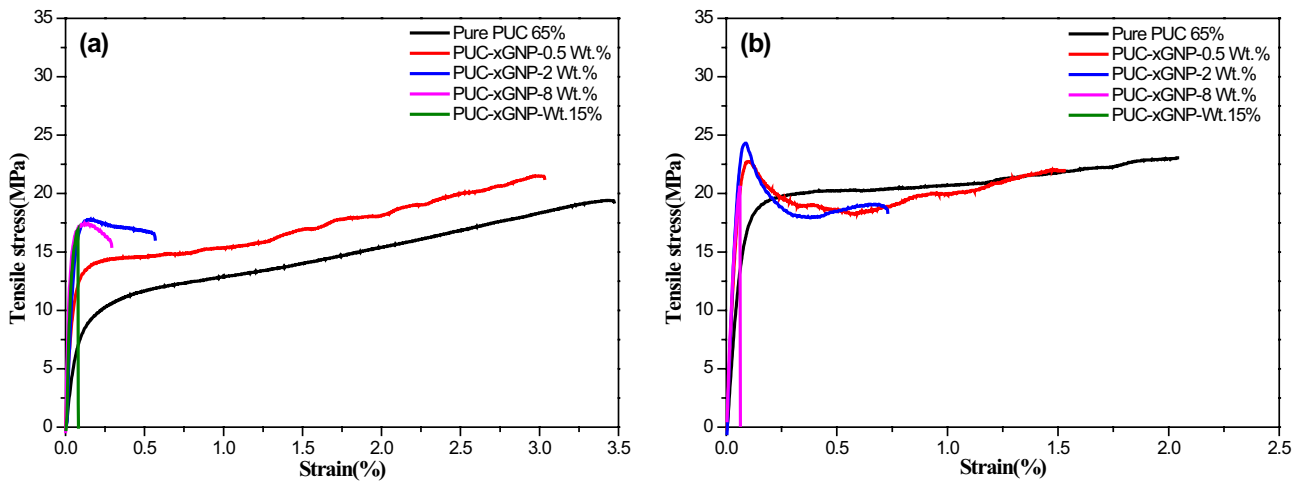


Fig. 8 Typical stress–strain data for conditioned (25 °C, 50% humidity), (a) non-annealed, and (b) annealed (80 °C for 4 days) samples of pure PUC and PUC-xGNP nanocomposites

key factor of adequate compatibility can create better and more uniform stress transfer. However, in the present case, this reduction in tensile properties after thermal treatment reflects the hypothesis of the restacking and aggregation tendency of xGNPs [71]. As is known, xGNP tends to aggregate through the addition of large amounts. The stress–strain curve of PUC/xGNP samples is represented the strength performance compared with pure PUC, three clear regions relevant to the microstructure of PUC were identified. The regions consist initially of the quasi-linear elastic deformation due to re-crystallisation and the ordering trend of hard segments. The second regime of the curve was observed as corresponding to the deformation of soft segments and represented as a plateau region in addition to some alignment of short ordered hard segments. Finally, the strain hardening region was observed, due to the crystallisation induced by the tensile loads and then the break-up of the PUC chains [72]. The advantages of the reinforcing effect exist when the effective interaction happened between the polymer–filler interface [73, 74].

Halpin–Tsai equations

The mechanical properties (elastic modulus) of nanofiller-reinforced composites can be estimated using different models that are enormously affected by the geometry, orientation, and volume fraction, as well as the elastic properties of both matrices and fillers. A defined H-T model prediction was employed to verify the mechanical performance of PUC/xGNP nanocomposites. A conventional comparison was assigned to a 3D random H-T model and a 2D H-T model. As is known, graphene is a perfect material with a higher aspect ratio (length to thickness) and thus has a

larger modulus compared to other fillers [75]. Dispersion and distribution of such kinds of xGNP play a crucial role in obtaining an efficient interaction between PUC and those xGNPs [76]. Thus, the main function for enhancement by the xGNP usage can be vanished due to aggregation tendency at certain limits addition [77]. This is reflected in the quality of the final resultant materials through increasing the thickness of this filler compared to similar lengths (diameter). Herein, an alternative calculation micromechanical model (H-T model) was used in order to predict the shape-fitting factor, which is directly relevant to the aspect ratio of stacked xGNP particles [33]. This model is developed from elasticity conditions, and is diverse and quite accurate in comparison with other models [33]. Theoretically, the modulus of the PUC/xGNP nanocomposites increases as E of xGNP increases. The highest and lowest modulus values were represented by the ‘P’ and ‘S’ lines, which related to longitudinal modulus and the transverse modulus. The equations used to estimate the filler modulus variation with respect to the results obtained from the realistic tensile test experiments are as follows [78]:

$$\frac{E_c}{E_m} = \frac{1 + \xi\eta V_f}{1 - \xi\eta V_f} \quad (2)$$

$$\text{where } \eta = \frac{(E_f/E_m) - 1}{(E_f/E_m) + \xi} \quad (3)$$

where E_f , E_m and E_c are the elastic modulus of the fillers, matrix and composites, respectively; V_f is the volume fraction of fillers; and ξ is the shape factor that depends directly on the filler geometry and loading direction. In general, $\xi = 2(L/d)$ for fibres, where L is the fibre length and d is the

fibre diameter, and $\xi = 2$ (L/t) for disc-like platelets, which are adopted in this study, where L is the GNP length and t is the GNP thickness [78]. The shape factor ξ , which relates to the aspect ratio of reinforcement, has provided good agreement with the longitudinal modulus; conversely, the transverse modulus was found to be comparatively insensitive to aspect ratio [33].

For composites with unidirectional or discontinuous fillers, the modified Halpin–Tsai models can predict the composite elastic modulus in the longitudinal (E_L) and transverse (E_T) directions according to the equations below:

$$E_L = E_m \left(\frac{1 + \xi \eta_L V_f}{1 - \eta_L V_f} \right) \quad (4)$$

$$E_T = E_m \left(\frac{1 + 2\eta_T V_f}{1 - \eta_T V_f} \right) \quad (5)$$

where the parameters η_L and η_T can be expressed in the following equations:

$$\eta_L = \frac{E_f/E_m - 1}{E_f/E_m + \xi} \quad (6)$$

$$\eta_T = \frac{E_f/E_m - 1}{E_f/E_m + 2} \quad (7)$$

To follow the modified Halpin–Tsai models, the below assumptions should be applied to PUC nanocomposites filled with xGNPs: i: Both xGNPs and PUC are isotropic and firmly bonded to each other; ii: the GNPs are asymmetrical, identical in shape and size, homogeneously dispersed and aligned; iii: the GNPs are fully exfoliated and perfectly oriented [66]. A clear difference between the

predicted modified Halpin–Tsai elastic moduli and the real behaviour of the PUC/xGNP system was observed. This outcome resulted from the optimised parameters that were assumed for the reinforcement mechanism [79]. However, to study the effects of filler direction within the PUC matrix, the modified Halpin–Tsai equations have been adjusted with respect to the probable filler direction, which may be 2D or completely 3D and which may be randomly oriented.

The modified Halpin–Tsai (MH-T) equations for 2D and 3D random orientations can be written as shown below:

$$\text{2D randomly oriented filler } E_c = \frac{3}{8} E_L + \frac{5}{8} E_T \quad (8)$$

$$\text{3D randomly oriented filler } E_c = \frac{1}{5} E_L + \frac{4}{5} E_T \quad (9)$$

In this study, the E_m of PUC is 0.19 GPa; the aspect ratio (L/t) of GNP-M15 is 1875 when L and t represent the length and average thickness of GNP, which were taken as 15 μm and 8 nm respectively according to the supplier specifications [80]. Finally, ξ was taken as $2(L/t)$; in this case, it is equal to 3750.

Figure 9 illustrates the comparison between predicted and experimental data of the elastic modulus of xGNP-reinforced PUC. From this figure, a deviation between the predicted and experimental values of the elastic modulus of nanocomposites can be clearly observed. The predicted theoretical modulus of PUC/xGNP increases with increasing E_f and V_f . In particular, it can be observed that the experimental results fit at $E_f = 300$ GPa at loading < 1 Wt.% and lie between 200 and less than 50 GPa at a loading of > 8 Wt.%. It can then be seen that this trend decreases upon further GNP at the highest loadings, equal to 15 Wt.%. This does not fit with experimental results at higher loadings due to xGNPs aggregating and being

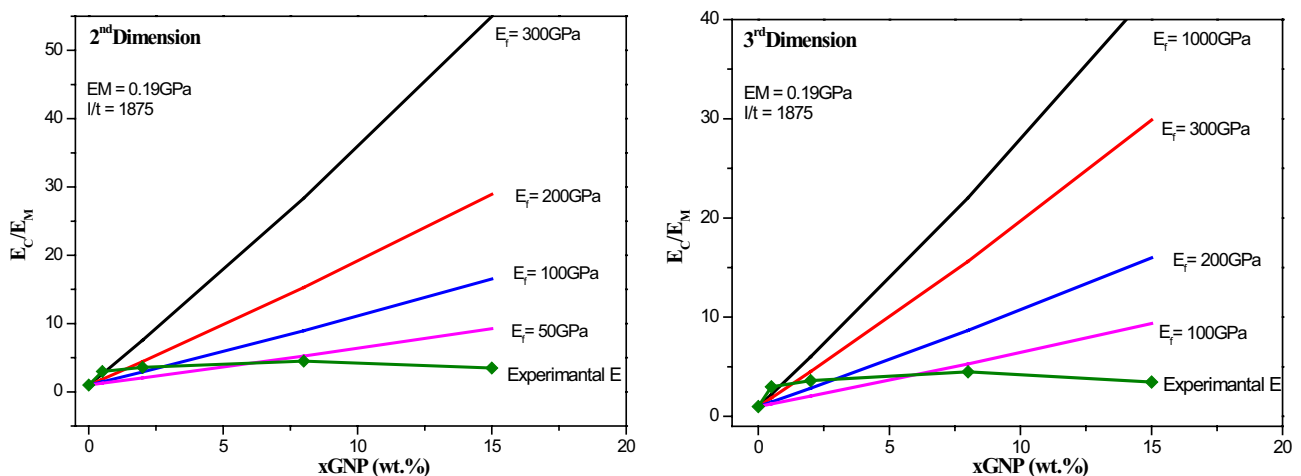


Fig. 9 The ratio of elastic modulus of PUC/xGNPs compared to neat PUC as a function of xGNP loading

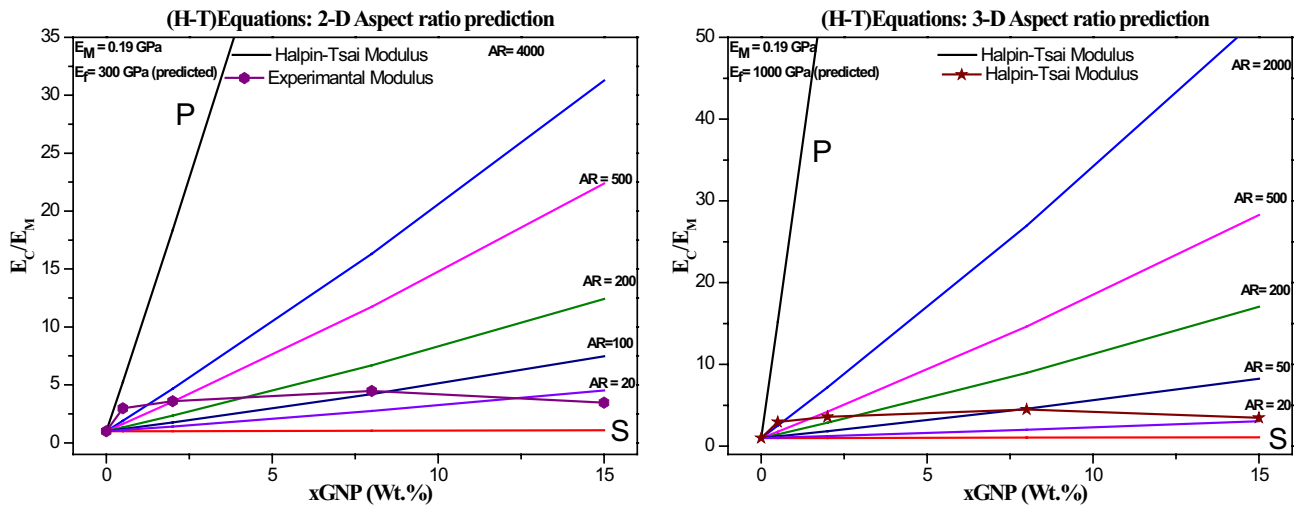


Fig. 10 The ratio of elastic modulus of PUC/xGNPs compared to neat PUC as a function of xGNP loading

randomly distribute [41]. However, further calculations using the 3D H-T model were conducted to demonstrate the optimised correlation via experimental data. It is clear that there is good agreement of filler moduli ($E_f = 1000\text{--}200$ GPa) between the calculated and experimental values for PUC nanocomposite modulus at lower GNP levels ($\leq 1\text{--}8$ Wt.%). Similarly to the 2D prediction, this trend is observed to reduce upon further GNP loadings. The reduction in E_f at high loading could be a result of non-homogeneity in dispersion, misalignment and size increments of the xGNP, resulting in the agglomeration or poor dispersion of nanofillers in the authentic behaviour of PUC/xGNP [81]. On the other hand, earlier work by M. M. Shokrieh et al. [82] reported the effective elastic modulus of GNP reinforced with epoxy polymer. The results of their study showed that non-uniform dispersion could be the major reason for divergence between the experimental and theoretical findings; this conclusion is compatible with the present results, in spite of the differences in GNP aspect ratio and processing methods.

As mentioned previously in these findings, the values of E_f at 300 GPa and 1000 GPa with respect to 2D and 3D predictions were selected to conduct further modelling to predict the elastic modulus of PUC/xGNP nanocomposites. This value will be extrapolated by varying the GNP aspect ratio (L/t) as shown in Fig. 10 with the assumption PUC moduli of 0.19 GPa. The lines marked U and L represent the calculations of predicted elastic modulus using the upper and lower bounds (series and parallel) of the rule of mixture models. A remarkable difference in both the 2D and 3D predictions of modulus have been observed, owing to the assumption of strong interface adhesion between xGNPs and the PUC matrix. Thus, the modulus seen was directly proportional to the ratio of L to t , which, it is suggested, can

be attributed to the poor dispersion, rolling up or folding of the GNP platelets as well as aggregation [41].

The correlation between the aspect ratio and modulus with respect to xGNP loading can be seen in Fig. 10. This relation reflects the status of xGNP exfoliation, since better exfoliation can result from an optimal mixing process and hence higher resultant modulus [83]. It was observed for the 2D estimation that at the essential minimum loading of GNPs (< 1 Wt.%) the empirical data matches with the line denoted as $L/t = 5000$ and then drops at a loading of > 1 Wt.% to lie exactly between $L/t = 500$ and even less than $L/t = 20$. At higher loading, the reduction in the aspect ratio of GNPs is in all probability due to the tendency of xGNPs to agglomerate and even to restack [84]. It is likely that the 3D calculation could be more accurate than the 2D model and thus better fit of prediction for the theoretical modulus based on the modified H-T equation [84].

Conclusions

PUC was considered a good candidate for many applications, and xGNPs were considered a useful reinforcement filler and inherently good modifier of the poorer properties of this PUC. Moreover, the architecture of PUC as a copolymer and the fact that its features are greatly affected by thermal treatment were the motivations to investigate the different properties with these two kinds of parameters. The incorporation of xGNPs increased most mechanical thermo-mechanical and thermal properties. The thermal and thermo-mechanical analysis including TGA and DMA displayed good thermal stability, and crystallinity increased due to xGNPs acting as a heterogeneous nucleation factor as well as possessing high barrier properties. Thermal transition was

also investigated by DSC thermograms to reveal the melting and crystallization peaks for PUC and their composites. In fact, the second scan of heating gave better thermal transition consistency due to erasure of the thermal history of PUC samples. On the other hand, the mechanical response of PUC filled with xGNPs was significantly raised according to the dispersion and interaction status. However, it was also of great importance to examine the effect of xGNPs on the microphase-separated structure of this polymer, which showed a positive effect on the final properties of the PUC/xGNP nanocomposites. A theoretical comparison was conducted to observe the aggregation tendency, especially at higher concentrations. The results showed that the increase in divergence corresponds to the increase in xGNP loadings.

Acknowledgements The authors are grateful to Materials Department at University of Kufa, Faculty of Engineering, for their unlimited support to achieve this research.

Funding This research received no specific grant from any funding agency or company.

Declarations

Conflict of Interest None.

References

1. Woods G (1990) The ICI Polyurethanes Book. 2nd edition edn. John Wiley and Sons, New York. <https://doi.org/10.1002/actp.1991.010420820>
2. Khudyakov IV, RDZaNT (2009) Polyurethane Nanocomposites. Des Monomers Polym 12:279–290. <https://doi.org/10.1163/15685509X448253>
3. Marcelo Antunes AC, Realinho V, Arencon D, Velasco JI (2014) Compression properties and cellular structure of polyurethane composite foams combining nanoclay and different reinforcements. International J Compos Mater 4:27–34. <https://doi.org/10.5923/j.cmaterials.201401.04>
4. Ahmadi Y, Ahmad S (2019) Recent progress in the synthesis and property enhancement of waterborne polyurethane nanocomposites: promising and versatile macromolecules for advanced applications. Polym Rev 60(2):1–41. <https://doi.org/10.1080/15583724.2019.1673403>
5. Albozahid M, Naji HZ, Alobad ZK, Saiani A (2021) Effect of OMMT reinforcement on morphology and rheology properties of polyurethane copolymer nanocomposites. J Elast Plast :009524432110061. <https://doi.org/10.1177/00952443211006160>
6. Albozahid M, Naji HZ, Alobad ZK, Saiani A (2021) Effect of OMMT reinforcement on morphology and rheology properties of polyurethane copolymer nanocomposites. J Elast Plast :009524432110061. <https://doi.org/10.1021/ma034604+>
7. Painter JMaP (2007) A Comparison of Hydrogen Bonding and Order in a Polyurethane and Poly(urethane-urea) and Their Blends with Poly(ethylene glycol). Macromolecules (40):1546–1554. <https://doi.org/10.1021/ma0626362>
8. Tian D, Wang F, Yang Z, Niu X, Wu Q, Sun P (2019) High-performance polyurethane nanocomposites based on UPy-modified cellulose nanocrystals. Carbohyd Polym 219:191–200. <https://doi.org/10.1016/j.carbpol.2019.05.029>
9. Xanthos M (2010) Functional Fillers for Plastics. Second, updated and enlarged edition edn. WILEY-VCH Verlag GmbH & Co. KGaA, Weinheim,
10. Hussein MA, Abu-Zied Bahaa M, Asiri AM (2018) Fabrication of EPYR/GNP/MWCNT carbon-based composite materials for promoted epoxy coating performance. RSC Adv 8(42):23555–23566. <https://doi.org/10.1039/c8ra03109f>
11. Byung Min Yoo HJS, Yoon HW, Park HB (2013) Graphene and graphene oxide and their uses in barrier polymers. J Appl Polym Sci. <https://doi.org/10.1002/app.39628>
12. Li B, Zhong W-H (2011) Review on polymer/graphite nanoplatelet nanocomposites. J Mater Sci 46(17):5595–5614. <https://doi.org/10.1007/s10853-011-5572-y>
13. Papageorgiou DG, Kinloch IA, Young RJ (2015) Graphene/elastomer nanocomposites. Carbon 95:460–484. <https://doi.org/10.1016/j.carbon.2015.08.055>
14. Young RJ, Kinloch IA (2012) Graphene and graphene-based nanocomposites. 1:145–179. <https://doi.org/10.1039/9781849734844-00145>
15. Albozahid MAMA (2018) Design of novel high modulus, tpus for nanocomposite applications University of Manchester the UK
16. Wang X, Hu Y, Song L, Yang H, Xing W, Lu H (2011) *In situ* polymerization of graphene nanosheets and polyurethane with enhanced mechanical and thermal properties. J Mater Chem 21(12):4222. <https://doi.org/10.1039/c0jm03710a>
17. Naz A, Kausar A, Siddiq M, Choudhary MA (2015) Comparative review on structure, properties, fabrication techniques, and relevance of polymer nanocomposites reinforced with carbon nanotube and graphite fillers. Polym-Plast Technol Eng 55(2):171–198. <https://doi.org/10.1080/03602559.2015.1055504>
18. Du J, Cheng H-M (2012) The fabrication, properties, and uses of graphene/polymer composites. Macromol Chem Phys 213(10–11):1060–1077. <https://doi.org/10.1002/macp.201200029>
19. Hassan AE-SM, EiD AI, El-Sheikh M, Ali WY (2017) Effect of graphene nanoplatelets and paraffin oil addition on the mechanical and tribological properties of low-density polyethylene nanocomposites. Arab J Sci Eng 43(3):1435–1443. <https://doi.org/10.1007/s13369-017-2965-5>
20. Yao KJMS, Hourston DJ, Luo DZ (2002) Polymer/ layered clay nanocomposites: 2 polyurethane nanocomposites. Polymer 43:1017–1020. [https://doi.org/10.1016/S0032-3861\(01\)00650-4](https://doi.org/10.1016/S0032-3861(01)00650-4)
21. Liu H, Huang W, Yang X, Dai K, Zheng G, Liu C, Shen C, Yan X, Guo J, Guo Z (2016) Organic vapor sensing behaviors of conductive thermoplastic polyurethane–graphene nanocomposites. J Mater Chem C. 4(20):4459–4469. <https://doi.org/10.1039/c6tc00987e>
22. Gurunathan T, Rao CRK, Narayan R, Raju KVS (2012) Polyurethane conductive blends and composites: synthesis and applications perspective. J Mater Sci 48(1):67–80. <https://doi.org/10.1007/s10853-012-6658-x>
23. Panahi-Sarmad M, Abrisham M, Noroozi M, Amirkiai A, Dehghan P, Goodarzi V, Zahiri B (2019) Deep focusing on the role of microstructures in shape memory properties of polymer composites: A critical review. Eur Polymer J 117:280–303. <https://doi.org/10.1016/j.eurpolymj.2019.05.013>
24. Bai JJ, Hu GS, Zhang JT, Liu BX, Cui JJ, Hou XR, Yu F, Li ZZ (2019) Preparation and rheology of isocyanate functionalized graphene oxide/thermoplastic polyurethane elastomer nanocomposites. J Macromole Sci Part B 58(3):425–441. <https://doi.org/10.1080/00222348.2019.1565102>
25. Solouki Bonab V, Maxian O, Manas-Zloczower I (2019) Carbon nanofiller networks- a comparative study of networks formed by branched versus linear carbon nanotubes in thermoplastic polyurethane. Polymer 175:227–234. <https://doi.org/10.1016/j.polymer.2019.05.031>

26. Yan Huan JL, Jie Wang, Fan Wu, Xiaoni Yang (2017) Physical properties and morphology of crosslinked polyurethane synthesized from para-phenylene diisocyanate and polyether polyol. *J Appl Polym Sci* 134 (37). <https://doi.org/10.1002/app.45241>
27. Zulkifli NNb, Badri KbH, Amin KAM (2016) Palm kernel oil-based polyester polyurethane composites incorporated with multi-walled carbon nanotubes for biomedical application. *Bioresources and Bioprocessing* 3 (1). <https://doi.org/10.1186/s40643-016-0102-z>
28. Anandhan S, Lee HS (2012) Influence of organically modified clay mineral on domain structure and properties of segmented thermoplastic polyurethane elastomer. *J Elastomers Plast* 46(3):217–232. <https://doi.org/10.1177/0095244312465300>
29. Dongxu Li GF, Xia H, Spencer PE, Coates PD (2015) Micro-contact reconstruction of adjacent carbon nanotubes in polymer matrix through annealing-induced relaxation of interfacial residual stress and strain. *J Appl Polym Sci*. <https://doi.org/10.1002/app.42416>
30. Yousefi N, Gudarzi MM, Zheng Q, Lin X, Shen X, Jia J, Sharif F, Kim J-K (2013) Highly aligned, ultralarge-size reduced graphene oxide/polyurethane nanocomposites: Mechanical properties and moisture permeability. *Compos A Appl Sci Manuf* 49:42–50. <https://doi.org/10.1016/j.compositesa.2013.02.005>
31. Lee C, Wei X, Kysar JW, Hone J (2008) Measurement of the elastic properties and intrinsic strength of monolayer graphene. *Science* 321(5887):385–388. <https://doi.org/10.1126/science.1157996>
32. Andrea Caradonna GC, Giorcelli M, Frache A, Badini C (2017) Thermal behavior of thermoplastic polymer nanocomposites containing graphene nanoplatelets. *J Appl Polym Sci*. <https://doi.org/10.1002/app.44814>
33. Ajorloo MF, Ohshima M, Taki M, Kentaro (2019) How are the thermal properties of polypropylene/graphene nanoplatelet composites affected by polymer chain configuration and size of nanofiller. *Mater Des* 181:108068. <https://doi.org/10.1016/j.matdes.2019.108068>
34. Karolina Gaska RK, Xiangdong Xu, Gubanski S, Müller C, Pandit S, Mokkaipati VRSS, Mijakovic I, Rybak A, Siwek A, Svensson M (2019) Highly structured graphene polyethylene nanocomposites. *AIP Conf Proc* 2065:030061. <https://doi.org/10.1063/1.5088319>
35. Xu W, Jambhulkar S, Verma R, Franklin R, Ravichandran D, Song K (2019) In situ alignment of graphene nanoplatelets in poly(vinyl alcohol) nanocomposite fibers with controlled stepwise interfacial exfoliation. *Nanoscale Advances* 1(7):2510–2517. <https://doi.org/10.1039/c9na00191c>
36. Gedler GA, Borca-Tasciuc M, Velasco T, Ozisik JI, R. (2016) Effects of graphene concentration, relative density and cellular morphology on the thermal conductivity of polycarbonate-graphene nanocomposite foams. *Eur Polymer J* 75:190–199. <https://doi.org/10.1016/j.eurpolymj.2015.12.018>
37. Huang A, Wang H, Ellingham T, Peng X, Turng L-S (2019) An improved technique for dispersion of natural graphite particles in thermoplastic polyurethane by sub-critical gas-assisted processing. *Compos Sci Technol* 182:107783. <https://doi.org/10.1016/j.compscitech.2019.107783>
38. Gupta RK, Hashmi SAR, Verma S, Naik A, Nair P (2020) Recovery Stress and Storage Modulus of Microwave-Induced Graphene-Reinforced Thermoresponsive Shape Memory Polyurethane Nanocomposites. *J Mater Eng Perform*. <https://doi.org/10.1007/s11665-020-04568-5>
39. Albozahid M, Habeeb SA, Ismael Alhilo NA, Saiani A (2020) The impact of graphene nanofiller loading on the morphology and rheology behaviour of highly rigid polyurethane copolymer. *Mater Res Express* 7(12):125304. <https://doi.org/10.1088/2053-1591/aba5ce>
40. Bera M, Maji PK (2017) Effect of structural disparity of graphene-based materials on thermo-mechanical and surface properties of thermoplastic polyurethane nanocomposites. *Polymer* 119:118–133. <https://doi.org/10.1016/j.polymer.2017.05.019>
41. Pashupati Pokharel HB, Jung-Gyu Lim, Kyoung Yong Lee, Sunwoong Choi (2015) Effects of titanate treatment on morphology and mechanical properties of graphene nanoplatelets/high density polyethylene nanocomposites. *J Appl Polym Sci* 132 (23):42073 (42071 of 42011). <https://doi.org/10.1002/app.42073>
42. Lin J, Zhang H, Tang M, Tu W, Zhang X (2014) Improved Thermal Property of a Multilayered Graphite Nanoplatelets Filled Silicone Resin Composite. *J Mater Eng Perform* 24(2):920–929. <https://doi.org/10.1007/s11665-014-1356-2>
43. Lin J, Zhang P, Zheng C, Wu X, Mao T, Zhu M, Wang H, Feng D, Qian S, Cai X (2014) Reduced silanized graphene oxide/epoxy-polyurethane composites with enhanced thermal and mechanical properties. *Appl Surf Sci* 316:114–123. <https://doi.org/10.1016/j.apsusc.2014.07.058>
44. Mahapatra SS, Yadav SK, Yoo HJ, Ramasamy MS, Cho JW (2014) Tailored and strong electro-responsive shape memory actuation in carbon nanotube-reinforced hyperbranched polyurethane composites. *Sens Actuators, B Chem* 193:384–390. <https://doi.org/10.1016/j.snb.2013.12.006>
45. Valentini L, Cardinali M, Kenny J (2014) Hot press transferring of graphene nanoplatelets on polyurethane block copolymers film for electroactive shape memory devices. *J Polym Sci, Part B: Polym Phys* 52(16):1100–1106. <https://doi.org/10.1002/polb.23539>
46. Bian J, Lin HL, He FX, Wei XW, Chang IT, Sancaktar E (2013) Fabrication of microwave exfoliated graphite oxide reinforced thermoplastic polyurethane nanocomposites: Effects of filler on morphology, mechanical, thermal and conductive properties. *Compos A Appl Sci Manuf* 47:72–82. <https://doi.org/10.1016/j.compositesa.2012.12.009>
47. Lei H, Liu Z, He C, Zhang S-C, Liu Y-Q, Hua C-J, Li X-M, Li F, Chen C-M, Cai R (2016) Graphene enhanced low-density polyethylene by pretreatment and melt compounding. *RSC Adv* 6(103):101492–101500. <https://doi.org/10.1039/c6ra15702e>
48. Dingchun Zhu YR, Liao G, Jiang S, Liu F, Guo J, Gaojie Xu (2017) Thermal and mechanical properties of polyamide 12/graphene nanoplatelets nanocomposites and parts fabricated by fused deposition modeling. *J Appl Polym Sci*. <https://doi.org/10.1002/app.45332>
49. Nguyen DA, Lee YR, Raghu AV, Jeong HM, Shin CM, Kim BK (2009) Morphological and physical properties of a thermoplastic polyurethane reinforced with functionalized graphene sheet. *Polym Int* 58(4):412–417. <https://doi.org/10.1002/pi.2549>
50. Han PJYaCD (2000) Effect of Thermal History on the Rheological Behavior of Thermoplastic Polyurethanes. *Macromolecules* (33):2171–2183. <https://doi.org/10.1021/ma991741r>
51. Bourque AJ, Locker CR, Tsou AH, Vadlamudi M (2016) Nucleation and mechanical enhancements in polyethylene-graphene nanoplate composites. *Polymer* 99:263–272. <https://doi.org/10.1016/j.polymer.2016.07.025>
52. Pielichowska K, Bieda J, Sztatkowski P (2016) Polyurethane/graphite nano-platelet composites for thermal energy storage. *Renew Energy* 91:456–465. <https://doi.org/10.1016/j.renene.2016.01.076>
53. Fahimeh Askari MB, Mohammad Barmar, Parvin Shokrollahi (2016) Polyurethane/amino-grafted multiwalled carbon nanotube nanocomposites: Microstructure, thermal, mechanical, and rheological properties. *J Appl Polym Sci* 134 (4):44411 (44411 of 44419). <https://doi.org/10.1002/app.44411>
54. Boubakri A, Haddar N, Elleuch K, Bienvenu Y (2011) Influence of thermal aging on tensile and creep behavior of thermoplastic polyurethane. *Comptes Rendus Mécanique* 339(10):666–673. <https://doi.org/10.1016/j.crme.2011.07.003>
55. Libanori R, Münch FHL, Montenegro DM, Studart AR (2012) Hierarchical reinforcement of polyurethane-based composites

- with inorganic micro- and nanoplatelets. *Compos Sci Technol* 72(3):435–445. <https://doi.org/10.1016/j.compscitech.2011.12.005>
56. Yadav SK, Cho JW (2013) Functionalized graphene nanoplatelets for enhanced mechanical and thermal properties of polyurethane nanocomposites. *Appl Surf Sci* 266:360–367. <https://doi.org/10.1016/j.apsusc.2012.12.028>
 57. Pokharel P, Choi S, Lee DS (2015) The effect of hard segment length on the thermal and mechanical properties of polyurethane/graphene oxide nanocomposites. *Compos A Appl Sci Manuf* 69:168–177. <https://doi.org/10.1016/j.compositesa.2014.11.010>
 58. Lin S, Anwer MAS, Zhou Y, Sinha A, Carson L, Naguib HE (2018) Evaluation of the thermal, mechanical and dynamic mechanical characteristics of modified graphite nanoplatelets and graphene oxide high-density polyethylene composites. *Compos B Eng* 132:61–68. <https://doi.org/10.1016/j.compositesb.2017.08.010>
 59. Liang JZ, Du Q, Tsui GCP, Tang CY (2016) Tensile properties of graphene nano-platelets reinforced polypropylene composites. *Compos B Eng* 95:166–171. <https://doi.org/10.1016/j.compositesb.2016.04.011>
 60. Taheri S, Sadeghi GMM (2015) Microstructure–property relationships of organo-montmorillonite/polyurethane nanocomposites: Influence of hard segment content. *Appl Clay Sci* 114:430–439. <https://doi.org/10.1016/j.clay.2015.06.036>
 61. Razeghi M, Pircheraghi G (2018) TPU/graphene nanocomposites: Effect of graphene functionality on the morphology of separated hard domains in thermoplastic polyurethane. *Polymer* 148:169–180. <https://doi.org/10.1016/j.polymer.2018.06.026>
 62. Pedrazzoli D, Manas-Zloczower I (2016) Understanding phase separation and morphology in thermoplastic polyurethanes nanocomposites. *Polymer* 90:256–263. <https://doi.org/10.1016/j.polymer.2016.03.022>
 63. Kishor Kumar Sadasivuni DP, Kumar B, Strankowski M, Ruth Cardinaels PM, Thomas S, Grohens Y (2014) Dielectric properties of modified graphene oxide filled polyurethane nanocomposites and its correlation with rheology. *Compos Sci Technol* 104:18–25. <https://doi.org/10.1016/j.compscitech.2014.08.025>
 64. Abbasi A, Mir Mohamad Sadeghi G, Ghasemi I, Shahrousvand M (2018) Shape memory performance of green *in situ* polymerized nanocomposites based on polyurethane/graphene nanoplatelets: Synthesis, properties, and cell behavior. *Polymer Composites* 39(11):4020–4033. <https://doi.org/10.1002/pc.24456>
 65. Hosseini-Sianaki T, Nazockdast H, Salehnia B, Nazockdast E (2015) Microphase separation and hard domain assembly in thermoplastic polyurethane/multiwalled carbon nanotube nanocomposites. *Polym Eng Sci* 55(9):2163–2173. <https://doi.org/10.1002/pen.24101>
 66. Chen Z, Lu H (2012) Constructing sacrificial bonds and hidden lengths for ductile graphene/polyurethane elastomers with improved strength and toughness. *J Mater Chem* 22(25):12479. <https://doi.org/10.1039/c2jm30517h>
 67. Gaikwad SD, Dravid SV, Sonawane BU, Abraham M, Goyal RK (2019) Dynamic mechanical and creep properties of poly(ether ketone)-graphite nanoplatelet (GNP) nanocomposites. *Polym Plast Technol Mater* 58(15):1691–1701. <https://doi.org/10.1080/25740881.2018.1563141>
 68. Zhang Y, Zhang Y, Liu Y, Wang X, Yang B (2016) A novel surface modification of carbon fiber for high-performance thermoplastic polyurethane composites. *Appl Surf Sci* 382:144–154. <https://doi.org/10.1016/j.apsusc.2016.04.118>
 69. Sahebi Jouibari I, Kamkar M, Nazockdast H (2017) Nanoparticle effects of thermoplastic polyurethane on kinetics of microphase separation, with or without preshear. *Polym Compos* 39(12):4551–4559. <https://doi.org/10.1002/pc.24563>
 70. Nautiyal P, Boesl B, Agarwal A (2017) Harnessing Three Dimensional Anatomy of Graphene Foam to Induce Superior Damping in Hierarchical Polyimide Nanostructures. *Small* 13(10). <https://doi.org/10.1002/sml.201603473>
 71. Wang Z, Li S, Wu Z (2015) The fabrication and properties of a graphite nanosheet/polystyrene composite based on graphite nanosheets treated with supercritical water. *Compos Sci Technol* 112:50–57. <https://doi.org/10.1016/j.compscitech.2015.03.010>
 72. Li X, Deng H, Li Z, Xiu H, Qi X, Zhang Q, Wang K, Chen F, Fu Q (2015) Graphene/thermoplastic polyurethane nanocomposites: Surface modification of graphene through oxidation, polyvinyl pyrrolidone coating and reduction. *Compos A Appl Sci Manuf* 68:264–275. <https://doi.org/10.1016/j.compositesa.2014.10.016>
 73. Sahoo NG, Jung YC, Yoo HJ, Cho JW (2006) Effect of functionalized carbon nanotubes on molecular interaction and properties of polyurethane composites. *Macromol Chem Phys* 207(19):1773–1780. <https://doi.org/10.1002/macp.200600266>
 74. Wang Y, Li T, Wang X, Ma P, Bai H, Dong W, Xie Y, Chen M (2016) Superior performance of polyurethane based on natural melanin nanoparticles. *Biomacromol* 17(11):3782–3789. <https://doi.org/10.1021/acs.biomac.6b01298>
 75. Kalaitzidou K, Fukushima H, Miyagawa H, Drzal LT (2007) Flexural and tensile moduli of polypropylene nanocomposites and comparison of experimental data to Halpin-Tsai and Tandon-Weng models. *Polym Eng Sci* 47(11):1796–1803. <https://doi.org/10.1002/pen.20879>
 76. Li B, Olson E, Perugini A, Zhong W-H (2011) Simultaneous enhancements in damping and static dissipation capability of polyetherimide composites with organosilane surface modified graphene nanoplatelets. *Polymer* 52(24):5606–5614. <https://doi.org/10.1016/j.polymer.2011.09.048>
 77. Ramin Shamsi MM, Mojtaba Koosha (2016) Synthesis of CNT-polyurethane nanocomposites using ester-based polyols with different molecular structure: Mechanical, thermal, and electrical properties. *J Appl Polym Sci* 134(10):44567 (44561 of 44513). <https://doi.org/10.1002/app.44567>
 78. Kardos JCHaJL (1976) The Halpin-Tsai Equations: A Review. *Polym Eng Sci* 16(5)
 79. Cai C, Liu L, Fu Y (2019) Processable conductive and mechanically reinforced polylactide/graphene bionanocomposites through interfacial compatibilizer. *Polym Compos* 40(1):389–400. <https://doi.org/10.1002/pc.24663>
 80. <http://www.sigmaldrich.com/>
 81. Zhong J, Isayev AI, Zhang X (2016) Ultrasonic twin screw compounding of polypropylene with carbon nanotubes, graphene nanoplates and carbon black. *Eur Polymer J* 80:16–39. <https://doi.org/10.1016/j.eurpolymj.2016.04.028>
 82. Shokrieh MM, Esmkhani M, Shahverdi HR, Vahedi F (2013) Effect of Graphene Nanosheets (GNS) and Graphite Nanoplatelets (GNP) on the Mechanical Properties of Epoxy Nanocomposites. *Sci Adv Mater* 5(3):260–266. <https://doi.org/10.1166/sam.2013.1453>
 83. Lijuan Zhao XS, Liu Qi, Zhao J, Xing W (2015) Natural Rubber/Graphene Oxide Nanocomposites Prepared by Latex Mixing. *Journal of Macromolecular Science, Part B* 54:581–592
 84. Ahmadi-Moghadam B, Taheri F (2014) Effect of processing parameters on the structure and multi-functional performance of epoxy/GNP-nanocomposites. *J Mater Sci* 49(18):6180–6190. <https://doi.org/10.1007/s10853-014-8332-y>

Publisher's Note Springer Nature remains neutral with regard to jurisdictional claims in published maps and institutional affiliations.